Open Ceramics 13 (2023) 100324

Contents lists available at ScienceDirect

Open Ceramics

journal homepage: www.sciencedirect.com/journal/open-ceramics

Electrospinning of ZrO_2 fibers without sol-gel methods: Effect of inorganic Zr-source on electrospinning properties and phase composition

Tony Lusiola [a], Arun Ichangi [a], Daniel Weil [a,b], Tutu Sebastian [a], Christos Aneziris [b], Thomas Graule [a,b], Frank Clemens [a,*]

[a] Laboratory of High Performance Ceramics, Empa, Swiss Federal Laboratories for Materials Science and Technology, Dübendorf, CH, Switzerland
[b] Institute of Ceramics, Glass and Construction Materials, Technische Universität Bergakademie Freiberg (D), Germany

ARTICLE INFO

Keywords:
Zirconia
Nanofibers
Electrospinning

ABSTRACT

The aim of this study was the electrospinning of zirconia nanofibers without sol-gel precursors. Low-cost Zr-oxide and Zr-carbonate inorganic materials, with high molecular Zr-content compared to sol-gel methods, were used for precursor formulation. Using a polyvinylpyrrolidone (PVP) polymeric binder, zirconia nanofibers could successfully be synthesised with both Zr-sources. The effects of different electrospinning parameters were investigated to stabilize the processing and reduce the deviation of nanofiber diameters. Fibres calcined at 1000 °C produced from the two different precursors displayed differing crystal phases of zirconia. The one based on nanoparticles revealed a significantly higher amount of tetragonal phase. Zirconia nanofibers with poly-granular microstructure across the diameter were successfully produced.

1. Introduction

Zirconia (ZrO_2) is an oxide ceramic that has been widely studied for its unique properties, like high fracture toughness, low toxicity and low corrosion potential [1–3]. These properties have ensured that zirconia finds usage in biomedical and mechanical applications [4,5]. In addition to the above-mentioned applications, nanoparticles of zirconia have been studied in applications as sensors and catalysts owing to their enhanced properties at the nanoscale [6,7].

To harness the unique material properties at the nanoscale, over the past few decades, a lot of work has been done on shaping the materials into anisotropic morphologies like nanoplates, nanorods and nanoparticles [8–10]. Among these, nanofibers present a fundamentally interesting opportunity to harness specific material properties owing to their high specific area and a high degree of anisotropic morphology [11,12]. Electrospinning enables the production of ceramic nanofibers with diameters ranging from tens of nanometers to microns using a mixture of polymers, metal alkoxides, or inorganic salts [13,14]. Additionally, electrospinning has also been explored for the preparation of nanoparticles and complex anisotropic morphologies like multichannel microtubes [15,16]. The electrospinning process contains numerous parameters (e.g. distance of the electrodes, electrical field, pumping speed, needle size, etc.) that affect the yield, shape and dimensions of spun fibers. Those parameters are influenced by solution properties like viscosity, electrical conductivity, surface tension, polymer molecular weight, metal salt source and content, moisture and stability of the slurry. Electrospun parameters and solution properties are often investigated in each study. However, the influence of different precursor raw materials on the final phase composition of the ceramic nanofibers are relatively unexplored. Herein, we attempt to address this knowledge gap by preparing Zirconium dioxide (ZrO_2) nanofibers with a choice of different starting precursor materials.

In this study, the synthesis of a non-woven zirconia nanofiber fabric with poly-granular microstructure was attempted via electrospinning. This study aimed to investigate the production of nanofibers using inorganic zirconia sources (oxides and carbonates) and their influence on the crystalline phase of the sintered nanofibers. Additionally, an investigation of typical electrospinning parameters was used to evaluate the flexibility of fiber diameters with multiple nano-sized grain structures. Additionally, the effect of the electrical conductivity of the precursor composition on processing and the diameter of fibers was investigated.

1.1. Overview of zirconia electrospinning formulations

In the literature, a wide range of precursor formulations to produce

* Corresponding author.
E-mail address: frank.clemens@empa.ch (F. Clemens).

https://doi.org/10.1016/j.oceram.2022.100324
Received 30 September 2022; Received in revised form 23 November 2022; Accepted 13 December 2022
Available online 17 December 2022
2666-5395/© 2022 The Authors. Published by Elsevier Ltd on behalf of European Ceramic Society. This is an open access article under the CC BY license (http://creativecommons.org/licenses/by/4.0/).

Table 1
Shows selected precursor formulations from literature used to produce zirconia fibers stating raw materials, average fiber diameters and stated applications.

Reference	Zr precursor	Binder	Solvent	e-spun fiber ø (μm)	Application
*Zhang et al. [17]	Zr-nanoparticles	PEO & PEG	H_2O & THF	0.45–0.7	High strength reinforcement & high-temperature insulation
*Sun et al. [18]	Zr-carbonate	PVP	DIW & acetic acid	0.4–0.6	Mechanical & electronic applications
*Li et al. [19]	Zr-nanoparticles	PVP	H_2O & ethanol	0.3	Mechanical & electronic applications
*Wycisk et al. [20]	Zr-nanoparticles	PVB	IPA & butanol	n/a	SO_2 gas adsorption
Shao et al. [21]	Zr-oxychloride	PVA	DIW	0.05–0.2	Nano- electronic & optoelectronic devices
Zhang et al. [22]	Zr-oxychloride	PVP	H_2O & ethanol	0.4–2	Support for active phase in catalytic combustion
Zhang et al. [23]	Zr-oxychloride	PVP	DIW & ethanol	1.2	Long-lasting phosphorescence energy storage
Jing et al. [24]	Zr-oxychloride	PVP	DIW & ethanol	0.04	Nano-material applications
Azad et al. [25]	Zr-oxychloride	PVP	DIW & ethanol	n/a	Optics, catalysis & data-storage
Lamastra et al. [26]	Zr-nanoparticles	PVA	DIW	0.6	Mechanical, thermal stability & reduced water solubility
Dharmaraj et al. [27]	Zr-isopropoxide	PVAc	DMF & ethanol	0.4–0.5	Electronics, photonics & sensing

Table 2
Shows the adjusted formulations which were used to synthesize electrospun ZrO_2 fibers.

PVP [wt%]	Ethanol [wt%]	ZrO_2 (Nyacol) [wt%]
5.86	11.67	82.46
PVP [wt%]	Ethanol, acetic acid & acetylacetone [wt%]	Zr-carbonate [wt%]
2.40	65.76	31.84

zirconia electrospun fibers have been reported, ranging from suspensions to sol-gel systems. Depending on the desired fiber composition, diameter, morphology and properties, different systems may be chosen. A few selected systems in which zirconia fibers were obtained are shown in Table 1. The marked (*) references reported zirconia fibers with polygranular microstructure.

From the literature overview on electrospun zirconia fibers (Table 1), polyvinyl pyrrolidone (PVP) is shown to be a very popular binder system. In our work, we used formulations based on the literature reports of Sun et al. [18] and Li et al. [19].

2. Experimental

2.1. Formulations for electrospinning of ZrO_2 fibers

In our study, two different formulations based on zirconia nanoparticles and zirconium carbonate as a metal source were used to synthesize zirconia fibers. To prepare the electrospinning solution, the organic binder, solvent, and Zr-source raw materials were mixed in the ratios listed in Table 2. After mixing, the solution was subjected to 30 s of ultrasonic treatment. Later, the solutions were magnetically stirred at room temperature for 5 h at 600 rpm and then left still for 2 days. Sedimentation was apparent, and only the upper, clear portion of the solution was used for electrospinning tests. The stirring time for both formulations was adjusted to ensure the complete dissolution of the organic binder, and it does not influence the final composition of the prepared nanofibers.

2.1.1. Zirconia nanoparticle system

Colloidal 5–20 nm ZrO_2 nanoparticles with a pH value of 3.5 and a viscosity of 10 cP (colloidal zirconium oxide, Nyacol Nanotechnology Inc.) was used as one of the zirconium source material. Polyvinylpyrrolidone [PVP, Mw: 1,300,000 (Sigma Aldrich 437190)] was mixed with the Nyacol nano-particle suspension and the viscosity was adjusted by locally sourced ethanol (Alcosuisse AG, A15-A).

2.1.2. Zirconium carbonate system

The chemicals for the second system included polyvinylpyrrolidone [PVP, Mw: 1,300,000 (Sigma Aldrich 437190)], zirconium(IV) carbonate hydroxide oxide (Sigma Aldrich 520217), acetic acid (Sigma Aldrich A6283), acetylacetone (Sigma Aldrich P7754) and ethanol. Zirconium carbonate was added to the solvent mixture while stirring, afterwards, PVP was added. After the 30s of ultrasonic treatment, the solutions were magnetically stirred for a 5 h and then left still for 2 days.

2.2. Electrical conductivity of the formulations

The electrical conductivity of the precursors and electrospinning solutions/suspensions was measured on a Metrohm 712 Conductometer (Metrohm AG, Switzerland) at room temperature.

2.3. Electrospinning of the formulations

The fiber mats were obtained by electrospinning using a NEU-Pro (NaBond Technologies Co., Limited - China) machine. The machine includes a drum-based fiber collector. The effect of process parameters (voltage, collection distance, needle gauge and flow rate) on fiber nanostructure and diameters were studied for both systems listed in Table 2. The prepared two different formulations were processed under different electrospinning conditions.

2.4. Fiber characterisation and thermal treatment

The green nanofiber mat structures and nanofiber microstructure were studied by using a scanning electron microscope (SEM, VEGA3 TESCAN, Czech Republic). The nanofiber diameters were measured using the Imagic IMS Client software (Imagic bildverarbeitung AG, Switzerland). Debinding was carried out at 600 °C while the zirconia nanofibers were calcined at 1000 °C for 1 h under an air atmosphere with a heating rate of 1 °C/min. XRD measurement was carried out on a PANalytical X'Pert PRO MPD (Netherlands) machine to study the crystalline structure of the nanofibers. The shrinkage of the nanofibers was calculated by subtracting the average fiber diameters after heat treatment from those before the heat treatment, and dividing this diameter difference by the raw diameter, as shown in Equation (1):

$$S = \frac{d_{green} - d_{calc}}{d_{green}} * 100\% \quad \text{Equation 1}$$

S is the shrinkage, d_{green} refers to the green average fiber diameter, and d_{calc} is the average fiber diameter after calcination. Rietveld refinement was performed on the calcined samples using the Xpert Highscore software to study the crystalline phase composition of the material.

3. Results & discussion

3.1. Electrical conductivity testing

The conductivities of the electrospinning solutions/suspension are very important, as the electrostatic charging of the fluid at the tip of the nozzle results in the formation of the Taylor cone. As a result, it has a strong effect on the electrospinning process, fiber diameter, shape, etc. In one report, it was stated that the diameter of the electrospun

Table 3
Displays the conductivities of various electrospinning formulations measured by various authors, including solvents, precursors and binders used as well as the ceramic where applicable.

Solvent	Precursors	Binder	Conductivity (μS/cm)	Ceramic	Ref.
DIW	zirconium acetate solution	PVA[a]	264	zirconia	[30]
n-propanol	zirconium(IV) n-propoxide	PVP	58	YSZ[b]	[29]
DIW	nickel(II) nitrate	PVP	601,000	NiO	
Ethanol	nickel(II) nitrate	PVP	5.41	NiO	
2-ME, IPA, n-propanol & citric acid	nickel(II) nitrate	PVP	3.28	NiO	
DIW & ethanol	zinc acetate	PVA	1150	ZnO	[31]
DIW	zinc acetate	PVA	5780	ZnO	
DMF, acetone, ethanol & acetic acid	titanium(IV) isopropoxide & palladium(II) chloride	PVP	45–67	PdO–TiO_2	[32]
Propanol	n/a	PVB[c]	1.64	n/a	[33]
Butanol	n/a	PVB	3.90	n/a	
DMF	n/a	PVB	10.52	n/a	
Ethanol	n/a	PVB	10.40	n/a	
Acetic acid	n/a	PVB	0.72	n/a	

[a] PVA – polyvinyl alcohol.
[b] YSZ – yttria stabilized zirconia.
[c] PVB – polyvinyl butyral.

Table 4
Shows the electrical conductivities of the electrospinning recipes used in this study.

Electrospinning solution/suspension system	Conductivity (μS/cm)
Zirconia nanoparticle system	11,584
Zirconium carbonate system	4306

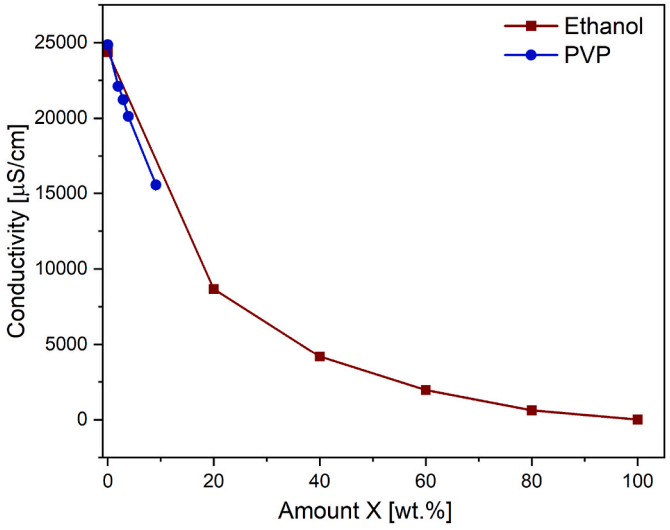

Fig. 1. Conductivity of ethanol (brown line) and PVP polymer (blue line) dispersed and stirred in colloidal zirconium oxide. X-axis represents the amount of ethanol and PVP mixed with colloidal zirconium oxide. (For interpretation of the references to colour in this figure legend, the reader is referred to the Web version of this article.)

nanofibers can be controlled by the electrical conductivity of the solution as the jet carry charges [28]. Unfortunately, conductivity is not often reported with the electrospinning of nanofibers. As shown in Table 3, the conductivity of different electrospinning formulations described in the literature can vary widely. In one report, it was noticed that the solution with very high conductivity of 601,000 μS/cm could not be electrospun [29]. Table 4 shows the conductivities of the two formulations which could be successfully electrospun in our work.

The nanoparticle-based electrospinning suspension showed a significantly higher conductivity in comparison to the carbonate-based system.

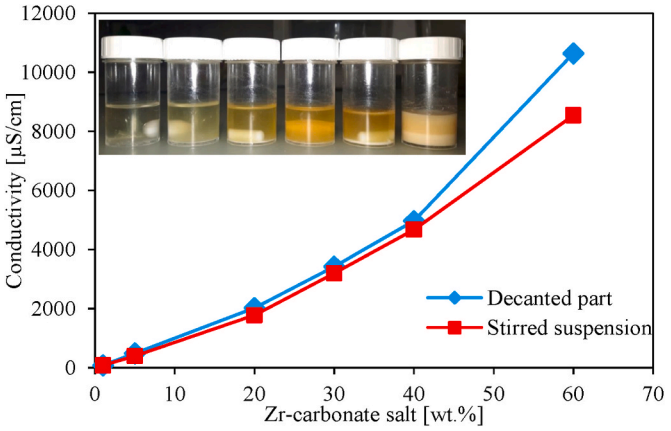

Fig. 2. Conductivity of partially dissolved zirconium(IV)-carbonate hydroxide oxide, the decanted portion (no sediment) and stirred portion with sediment suspended.

3.1.1. *Zirconia nanoparticle system*

The conductivity of the zirconia nanoparticle system was mainly dictated by the electrical conductivity of pure colloidal zirconium oxide (25,000 μS/cm), while the conductivity of ethanol has a value 2.5 μS/cm and the dissolved PVP had no discernible effect, as can be seen from Fig. 1. In general, electrospun nanofibres with the smallest fiber diameter can be obtained from the solution with the highest conductivity and vice versa (see SI, Fig. S1 for further details).

3.1.2. *Zirconium(IV)-carbonate system*

The conductivity in the zirconium carbonate system was greatly affected by the amount of zirconium carbonate. In general, the electrical conductivity of the electrospinning suspensions ranged from about 2400 to 3600 μS/cm, depending on the amount of the carbonate salt. To distinguish the effect of the sediments on conductivity, suspensions were made with 6 different zirconium(IV)-carbonate concentrations. The suspensions were stored for a few days to achieve full sedimentation. The upper, clear part (i.e. dissolved part) was decanted and the conductivity measured. The decanted samples were re-mixed with the sediments and the conductivity was measured (Fig. 2).

As expected, Fig. 2 shows that an increase in the amount of zirconium(IV)-carbonate salt results in an increase in the electrical conductivity in both experiments. No significant difference between the decanted and the dispersed system was observed. It can be assumed that an increase in conductivity with increased amounts of salt can be attributed to the higher concentration of free ions and other species susceptible to ionisation.

3.2. *Electrospinning*

Electrospinning was conducted with the two different formulations. The experiments were focused on the homogeneity of the electrospun fiber mat, e.g. fiber diameter, microstructure and morphology.

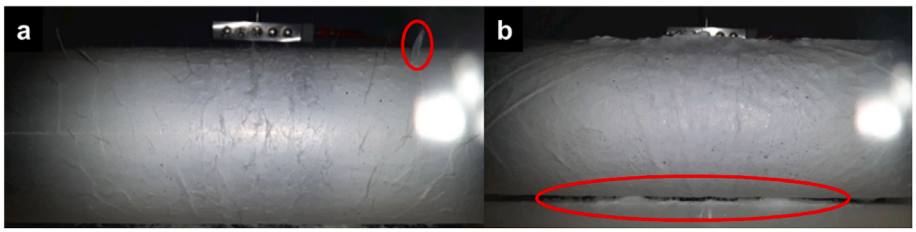

Fig. 3. a) image shows inhomogeneous mat with standing fibers, b) as well as accumulated fibers ripped from the collector caught between the cylindrical collector and machine base.

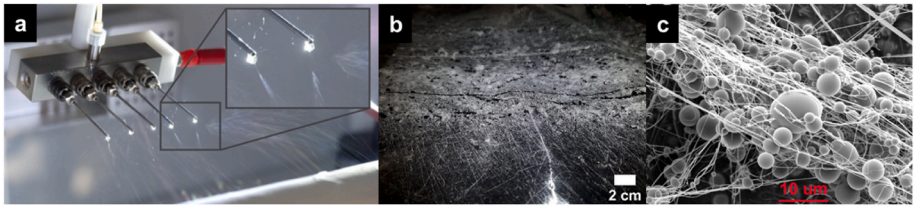

Fig. 4. Nanoparticle system; a) single and multi-jets emitted; b) prominent drops observed on the mat that dissolved already deposited fibers; c) bead formation using PVA and higher ethanol content.

3.2.1. *Zirconia nanoparticle system*

For the zirconia nanoparticle system, electrospinning was performed using flow rates ranging from 1 to 10 mL/h, voltages between 8 and 25 kV and needle to drum distances of 5 and 10 cm. The process was optimized by tuning in the composition as well as the electrospinning parameters i.e. voltage, distance, needle gauges and flow rate.

With a PVP amount of 4 wt % and above, needle clogging was observed, and the high conductivity of the precursor system caused the 'standing fiber' phenomenon which ended up being ripped off (Fig. 3).

The attribution of the standing fiber phenomenon to conductivity was due to the observation that when the electrical voltage was switched off the fibers would lie on the collector (Fig. 3b), but when turned on they would stand. From Gazquez et al. it is understood that dampening the conductivity of the solution would have enabled the collection of a homogeneous mat [34]. Normally during electrospinning, a single jet is emitted per needle, which is initially in a stable phase and then transients into the "whipping instability-zone". Sometimes though, multiple jets are ejected especially when the applied voltage is high. In the system with colloidal ZrO_2 nanoparticles, this proved to be true for applied voltages above 18 kV (Fig. 4a). The effect was however not permanent, the jet was switching back and forth from a single to multiple fibers during the spinning process. This can be explained by the rapid physical movement of the jet in the air, leading to varying electric potential.

Another issue of interest was the formation of droplets on the mat (Fig. 4b), which happened more frequently when distances between the collector and needles were lower than 10 cm. This effect also occurred when the flow rate was too high and/or when the amount of PVP was too low (low viscosity). This can be explained by the electrical field drawing the solution from the needles, combined with a low solution viscosity. Due to gravity and the electrical field, the jet was thinned to the extent the viscosity forces cannot retain the fiber form, resulting in the lowering of the surface area by the formation of droplets. Due to their electrical conductivity and inertia, they are still accelerated toward the collector and can reach the collector when using small distances. The main properties that influence droplet formation are viscosity, solution conductivity, solvent evaporation, surface tension and solubility of the polymer [35]. A further disadvantage of the droplet reaching the mat is that the solvent can dissolve the fibers already collected on the collector. Furthermore, lower than optimal viscosity led to the formation of beads as shown in Fig. 4c.

3.2.2. *Zirconium(IV)-carbonate system*

For the zirconium(IV)-carbonate system, electrospinning was successful between 14 and 25 kV, electrode distances between 5 and 12.5 cm and flow rates ranging from 2 to 10 mL/h. Besides varying the PVP amount from 2.4 to 6 wt %, 31 to 50 wt % zirconium (IV)-carbonate was added to investigate the effect on the electrospinning process. Before electrospinning, the formulations were always stored for a few days to achieve full sedimentation. Only the sediment-free part, separated by decanting, was used for the following studies. The electrospinning

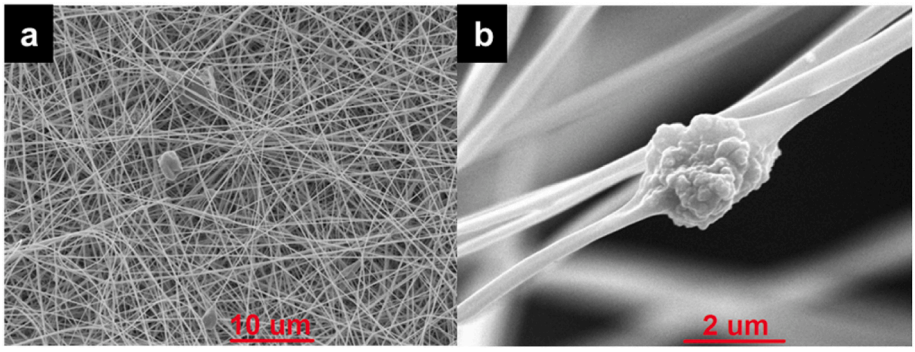

Fig. 5. Electrospun fibers produced using electrospinning solution that did not fully sediment, i.e. the Sun et al. -based system showing particles; a) between and b) in fibers.

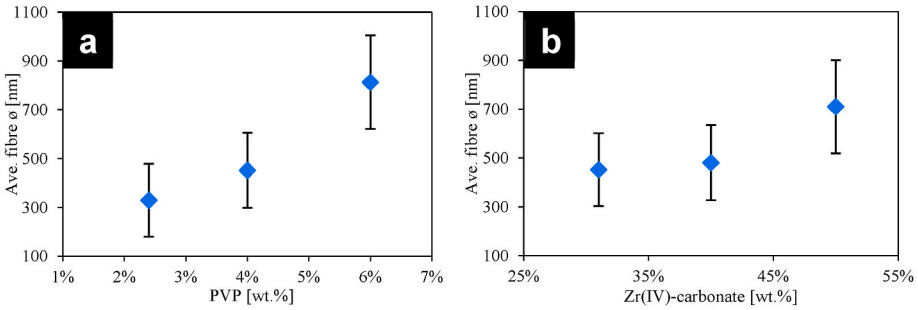

Fig. 6. Average nanofiber diameters of electrospinning solutions using different amounts of; a) PVP; b) zirconium carbonate salt.

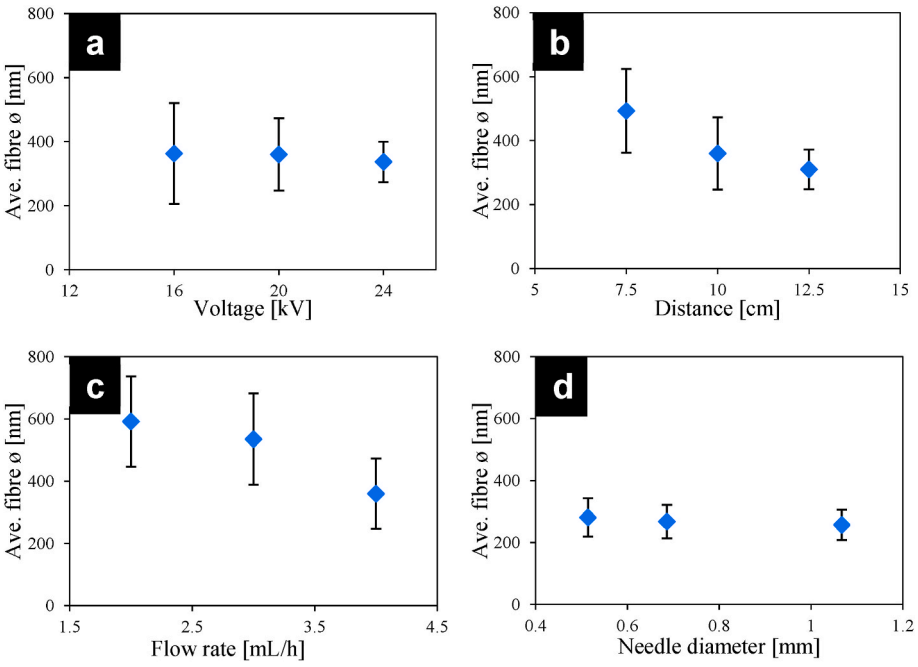

Fig. 7. Graphs showing the trends of average green nanofiber diameter with respect to changes in electrospinning parameters such as a) varying voltages; b) varying needle-to-collector distances; c) for different flow rates; d) varying needle diameters. (For interpretation of the references to colour in this figure legend, the reader is referred to the Web version of this article.)

experiments with the Sun et al..-based formulations yielded the best electrospinning results from all the tested systems [18]; a homogeneous mat was formed and spinning was consistent at voltages between 8 and 25 kV while using distances between 5 and 12.5 cm. All solutions made could be successfully electrospun. If the sedimentation and decanting step was not successful, particles were obtained in the electrospun mat (Fig. 5).

The results allowed further testing of processing parameters, by varying the precursors, flow rate, voltage, the distance between the needle and collector and needle gauge.

3.2.2.1. Varying amounts of PVP and zirconium salt. The effect of varying PVP and zirconium salt concentrations in the electrospinning solution on the green fiber diameters is shown in Fig. 6. One parameter was changed at a time, while the others were kept constant. These constant parameters were a voltage of 20 kV, a distance between needle and collector of 10 cm, a flow rate of 4 mL/h and a needle gauge of 17 (ø 1.067 mm). The error bars indicate the standard deviation of the nanofiber diameters measured by the SEM and give a hint about the distribution of nanofiber sizes.

With an increase in the amount of PVP, the diameters increased. But the 17-gauge needles were clogging more often with 6 wt % PVP indicating a high viscosity and thus the upper limit of the polymer binder amount for this needle size. As the electrospinning processing worked best at 4 wt % of PVP, this binder to solvent ratio was maintained. The electrospinning worked well with all amounts of zirconium(IV)-carbonate investigated i.e. up to 50 wt %. The diameters increased with the increasing amount of salt, as shown in Fig. 6 b. Also, the standard deviation of the nanofiber diameters decreased, to 33, 32 and 27% respectively, implying more uniform nanofiber mats. To achieve the highest ZrO_2 yield possible after heat treatment and because the electrospinning worked well, the 50 wt % zirconium(IV) carbonate composition was used further in different parameter-changing experiments.

3.2.2.2. Effect of electrospinning parameters on green fiber diameters. Experiments were carried out with the zirconium(IV) carbonate system to investigate how voltage, the distance between needle and collector, flow rate and needle diameter affect the green fiber diameters. These results are shown in Fig. 7.

3.2.2.3. Effect of voltage. Demir et al. suggested that the final diameter of the fibers under constant current flow depended on the applied voltage [36], with He et al. suggesting that fiber diameter has an allometric relationship to the applied voltage as shown in Equation (2) [37]:

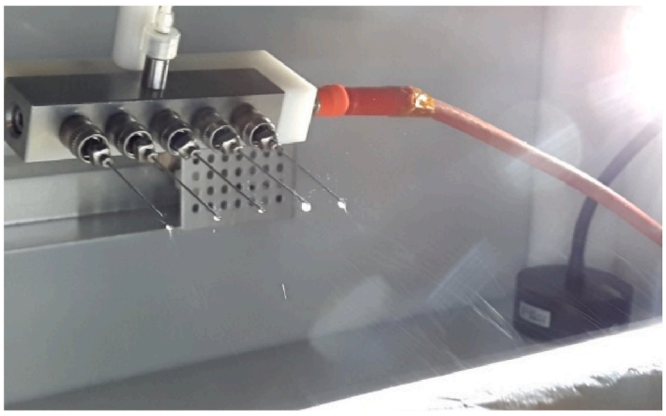

Fig. 8. Electrospinning showing drops formed at the needle tips in place of Taylor cones.

$d \approx$ E−0.5 Equation 2

Where d is the green fiber diameter and E is the applied electric field and thus predicts that increasing electrical fields result in smaller diameter fibers [38]; which has been found by several other groups [28, 39]. **Error! Reference source not found.**a shows that the average nanofiber diameter does not decrease significantly if we consider the diameter distribution of the green nanofibers. However, the standard deviation decreases significantly suggesting the production of finer and more uniform nanofibers, a trend also seen by Angammana et al. [28]. The stronger electrical field means an increase in the electrostatic repulsive force on the charged jet, favoring the narrowing of nanofiber diameter.

3.2.2.4. Needle-collector distance. The structure and morphology of electrospun fibers are easily affected by the electrospinning distance because of their dependence on the deposition time, solvent evaporation rate and whipping or instability interval [40]. **Error! Reference source not found.**b shows the relationship between nanofiber diameters and electrospinning distance. It is apparent that the diameters decrease with an increase in the needle-collector distance. Other authors have also found similar results [41,42], with the reason being that in general, the trend in fiber diameter follows that of the applied voltage because as the distance is increased the electrical field energy is reduced, and at the same time due to the larger distance that the jets must travel while in air, they get subjected to a stronger thinning and more solvent evaporates.

3.2.2.5. Flow rate. The flow rate is an important process parameter as it influences the jet velocity and the material transfer rate; with the advantage of a lower flow rate being the ability to allow sufficient solvent evaporation [43]. The fiber diameters decreased when electrospinning with a higher flow rate (**Error! Reference source not found.** c), which is the opposite of what has been documented in the literature [42,44,45]. This may be explained by the intermittent electrospinning observed with the lower flow rates resulting in higher solvent evaporation. The lower flow rates were too low to support consistent electrospinning. The needle diameter used in this work was relatively large 17 (ø 1.067 mm) compared to the standard needle gauge used in literature. The Taylor cone did not emerge directly from the needle, but rather out of a drop formed at the tip, as shown in Fig. 8. It was observed with the lower flow rates that first a drop would form at the needle tip, after which the Taylor cone would appear (spinning commences) and then disappear again, at which point spinning would stop. This process repeats itself after a new drop is formed following the flow rate. These drops meant that a bigger total suspension surface area was exposed when compared to smaller diameter needles. It is thought that due to having a relatively high surface area compared to their volume (when compared to a Taylor cone emerging from a smaller needle); more solvent was able to evaporate affecting the trend in fiber diameter due to the intermittent nature of the electrospinning.

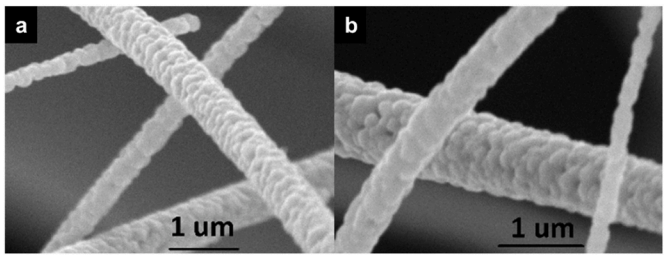

Fig. 9. Calcined fibers from the; a) zirconia nanoparticle system; b) zirconium (IV)-carbonate system.

3.2.2.6. Needle gauge. The 17-gauge needle with a larger diameter (ø 1.067 mm) was used as the standard because it made the electrospinning process much easier and stable, with less clogging compared to smaller needle gauges. From the results shown in **Error! Reference source not found.**d, using a higher needle gauge (smaller inner diameter) caused the fiber diameters to slightly increase. However, at first, this seems contradictory; a larger diameter should allow more suspension to flow through and before the experiments, it was expected that a bigger needle would cause an increase in the fiber diameters.

A possible explanation for this effect is the surface area of the solution. When the needle diameter is larger, the capillary forces on the tip change in such a way that the drop forming is bigger. A larger drop has a higher surface tension, possibly reducing the evaporation of the solvent. When spinning with smaller needles, a Taylor cone would form directly at the needle tip unlike with needle gauge 17 (Fig. 8). The cone forming from the bigger droplets (large needles) was smaller than the one coming directly from the needle tip (small diameter needles), possibly allowing more solvent evaporation and thus causing larger fiber diameters due to increased viscosity. The standard deviation changed from 19, 20–22% when using needle gauges 17, 19 and 21 respectively. This correlates with the electrospinning experience: when using a smaller diameter needle clogging happened more often, causing irregularities in the process. In this case, needle clogging was not a problem, but still meant a lower probability of having a stable process.

3.3. Heat treatment

Gazquez et al. found that sintered fiber diameters were primarily dependent on the equivalent solid content after thermal annealing [34]. Although high conductivity might result in thinner green fibers, the influence of solution conductivity on fiber diameter after annealing was found to be much less prominent than the solid content. All fibers were calcined for 1 h at 1000 °C.

The observed fiber morphology is in good agreement with the study reported by Li et al. [19] However, a further morphological comparison was not possible due to the low resolution of the SEM images.

3.3.1. Zirconia nanoparticle system

With the zirconia nanoparticle system, fibers obtained had the “necklace/bamboo” effect (Fig. 9a). After heat treatment, a shrinkage of 30% could be obtained. The fiber sizes ranged between 0.3 and 35 μm for the same process parameters. This results in standard deviations between 84 and 178%.

3.3.2. Zirconium(IV)-carbonate system

While using a low amount of PVP, the zirconium(IV)-carbonate system showed similar results in comparison with the zirconia nanoparticle, i.e. necklace effect. An increase in the volume of PVP resulted in

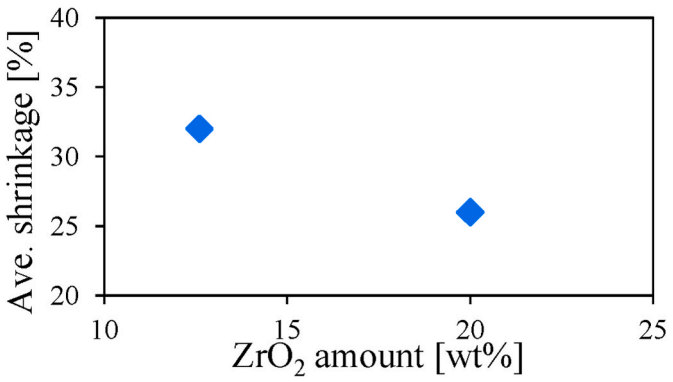

Fig. 10. The average shrinkage is influenced by the amount of ZrO_2 in modified Sun et al. based formulations.

larger fiber diameters and a poly-granular fiber morphology was obtained (Fig. 9b). Depending on the zirconia carbonate content the shrinkage after heat treatment varied between 27 and 34%. The average diameters ranged from 120 to 340 nm with a standard deviation of 78 nm. Fig. 10 shows how the shrinkage is affected by the Zr-precursor solids loading. The ZrO_2 content was calculated from the number of moles contained in the zirconium carbonate source. As expected, a higher loading yields a lower relative shrinkage.

3.4. Phase composition

Fig. 11 shows the X-ray diffractogram of the calcined samples and their phase analysis. It can be noted that both the calcined samples show mixed phases of monoclinic and tetragonal structures. Typically sintering at a temperature above 700 °C, the monoclinic phase dominates in electrospun fiber [19]. To quantify the different phases in the calcined nanofiber, Rietveld refinement was performed on the samples (see SI, Table S1). From the Rietveld refinement, it was estimated that the zirconia nanofibers prepared using the zirconium(IV)-carbonate system had an overwhelming monoclinic phase (Ref. code 01-080-0966) of about 92.2% and the rest being the tetragonal phase (Ref. code 01-079-1763). Interestingly, in the case of nanofibers prepared using the ZrO_2 nanoparticles colloid system, the tetragonal phase was at 82.8% and the monoclinic at 17.2%. This is in contrast to the work reported by Li et al. [19]. At 800 °C they observed a mainly monoclinic phase and at 1000 °C the structure had completely transformed into a pristine monoclinic phase. The main difference between the two studies is the heat treatment. While Li et al. used a high-temperature differential scanning calorimeter (HTDSC) with a heating rate of 10 °C/min, in our study we used a conventional furnace with a heating rate of 1 °C/min and a dwell time of 1 h. Due to the lower heating rate and a dwell time of 1 h, in our study a larger crystallite size can be expected. Based on these results, it can be concluded that the formation and transformation of crystalline phases of zirconia depend on several synthetic parameters including the type of precursor, doping with ions and the technique used for its synthesis and the followed post-thermal treatments. In one report, Sebastian et al. observed that the choice of polymer binder material influenced the final crystalline phase composition of electrospun hydroxyapatite fibers [46].

4. Conclusion

Two low-cost electrospinning systems, namely zirconium oxide nanoparticles and zirconium(IV) carbonate, have been investigated for the electrospinning of ZrO_2 fibers. The zirconia nanoparticle system was attempted with an initial issue being 'standing' fibers on the collector. A large variation of fiber diameter from nano to micrometer range has been observed which might be critical for some industrial applications. It was possible to synthesize zirconia fibers with a cheaper and easier method than using sol-gel precursors. The zirconium(IV)-carbonate system proved to work best regarding processing parameters, uniformity of fibers, and also reproducibility. Due to the relatively low standard deviations in the measured fiber characteristics, the zirconium(IV)-carbonate based system was selected for a further study concerning the influence of various parameters on fiber diameters and morphology. The solubility and visual inspection results of the various systems showed that both, solutions and suspension may successfully be used to produce electrospun zirconia fibers. With the zirconium(IV)-carbonate system, the fiber diameters could be varied easily by changing the amount of PVP and/or the zirconium(IV)-carbonate salt concentration. Suspensions with PVP amount from 2.4 wt % to 6 wt % and zirconium(IV)-carbonate amount up to 50 wt % were successfully spun. As the amount of binder and salt in the precursor was increased, larger average

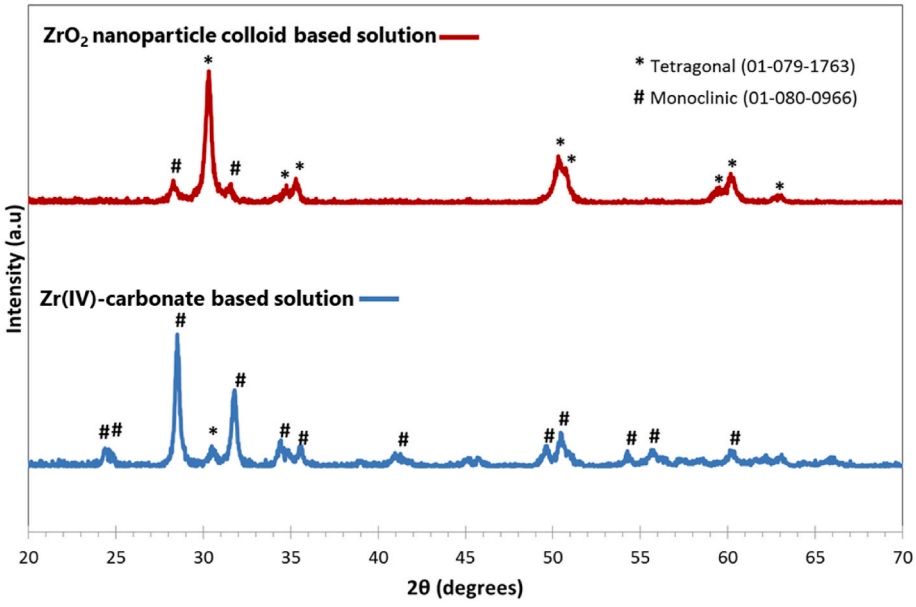

Fig. 11. X-ray diffraction patterns of calcined ZrO_2 nanofibers from the zirconia nanoparticle system and zirconium carbonate system, showing different crystalline phases.

green fiber diameters were obtained. In addition, the effect of voltage, distance, flow rate and needle gauges on fiber diameter was investigated in a certain range. Calcining the fibers at 1000 °C revealed a predominant monoclinic phase for the zirconium(IV)-carbonate system whereas a predominantly tetragonal phase with a minority monoclinic phase for the zirconia nanoparticle system was observed. Based on the fact, that polymeric binder (PVP) and solvent (ethanol) were kept constant in this study, it is obvious that the difference in phase composition is related to the different Zr-source. Increasing PVP binder or content of zirconium (IV)-carbonate salt, fibers with poly-granular microstructure across the nanofiber was successfully produced.

Declaration of competing interest

The authors declare that they have no known competing financial interests or personal relationships that could have appeared to influence the work reported in this paper.

Acknowledgment

The authors would like to thank the Collaborative Research Center 799 “TRIP-Matrix Composites” of the German Research Foundation for supporting this contribution in terms of Subproject A01.

Appendix A. Supplementary data

Supplementary data to this article can be found online at https://doi.org/10.1016/j.oceram.2022.100324.

References

[1] I. Denry, J.R. Kelly, State of the art of zirconia for dental applications, Dent. Mater. 24 (3) (2008) 299–307.
[2] I. Dion, et al., Physico-chemistry and cytotoxicity of ceramics: Part I–Characterization of ceramic powders, J. Mater. Sci. Mater. Med. 8 (5) (1997) 325–332.
[3] Y.-W. Chen, et al., Zirconia in Biomedical Applications. Expert Review of Medical Devices, vol. 13, 2016, pp. 945–963, 10.
[4] X. Zhang, X. Wu, J. Shi, Additive manufacturing of zirconia ceramics: a state-of-the-art review, J. Mater. Res. Technol. 9 (4) (2020) 9029–9048.
[5] H. Tanaka, et al., Mechanical properties of partially stabilized zirconia for dental applications, Journal of Asian Ceramic Societies 7 (4) (2019) 460–468.
[6] J.L. Gole, et al., Unique properties of selectively formed zirconia nanostructures, Adv. Mater. 18 (5) (2006) 664–667.
[7] S. Zhuiykov, N. Miura, Development of zirconia-based potentiometric NOx sensors for automotive and energy industries in the early 21st century: what are the prospects for sensors? Sensor. Actuator. B Chem. 121 (2) (2007) 639–651.
[8] L. Shi, et al., Photoluminescence and photocatalytic properties of rhombohedral CuGaO2 nanoplates, Sci. Rep. 6 (1) (2016) 1–10.
[9] Z. Ye, et al., Na-doped ZnO nanorods fabricated by chemical vapor deposition and their optoelectrical properties, J. Alloys Compd. 690 (2017) 189–194.
[10] M. Saravanan, et al., Green synthesis of anisotropic zinc oxide nanoparticles with antibacterial and cytofriendly properties, Microb. Pathog. 115 (2018) 57–63.
[11] J. Xue, et al., Electrospinning and electrospun nanofibers: methods, materials, and applications, Chem. Rev. 119 (8) (2019) 5298–5415.
[12] M. Hedayati, et al., BaTiO3 nanotubes by co-axial electrospinning: Rheological and microstructural investigations, J. Eur. Ceram. Soc. 40 (4) (2020) 1269–1279.
[13] A. Ichangi, et al., Li and Ta-modified KNN piezoceramic fibers for vibrational energy harvesters, J. Eur. Ceram. Soc. 41 (15) (2021) 7662–7669.
[14] L. Fei, et al., Electrospun bismuth ferrite nanofibers for potential applications in ferroelectric photovoltaic devices, ACS Appl. Mater. Interfaces 7 (6) (2015) 3665–3670.
[15] N. Radacsi, et al., Spontaneous formation of nanoparticles on electrospun nanofibres, Nat. Commun. 9 (1) (2018) 1–8.
[16] Y. Zhao, X. Cao, L. Jiang, Bio-mimic multichannel microtubes by a facile method, J. Am. Chem. Soc. 129 (4) (2007) 764–765.
[17] H. Zhang, M. Edirisinghe, Electrospinning zirconia fiber from a suspension, J. Am. Ceram. Soc. 89 (6) (2006) 1870–1875.
[18] G.-X. Sun, et al., Electrospun zirconia nanofibers and corresponding formation mechanism study, J. Alloys Compd. 649 (2015) 788–792.
[19] L. Li, et al., Phase transformation and morphological evolution of electrospun zirconia nanofibers during thermal annealing, Ceram. Int. 36 (2) (2010) 589–594.
[20] R. Wycisk, et al., Electrospun zirconium hydroxide nanoparticle fabrics as sorptive/reactive media, Adsorption 20 (2) (2014) 261–266.
[21] C. Shao, et al., A novel method for making ZrO2 nanofibres via an electrospinning technique, J. Cryst. Growth 267 (1–2) (2004) 380–384.
[22] Y. Zhang, et al., Preparation of CeO2–ZrO2 ceramic fibers by electrospinning, J. Colloid Interface Sci. 307 (2) (2007) 567–571.
[23] D. Zhang, et al., One dimensional Ti-doped zirconia wires prepared by electrospinning: characterization, morphology and photophysical features, J. Lumin. 157 (2015) 338–343.
[24] N. Jing, M. Wang, J. Kameoka, Fabrication of ultrathin ZrO< sub. 2 nanofibers by electrospinning, J. Photopolym. Sci. Technol. 18 (4) (2005) 503–506.
[25] A.-M. Azad, T. Matthews, J. Swary, Processing and characterization of electrospun Y2O3-stabilized ZrO2 (YSZ) and Gd2O3-doped CeO2 (GDC) nanofibers, Mater. Sci. Eng., B 123 (3) (2005) 252–258.
[26] F. Lamastra, et al., Nanohybrid PVA/ZrO2 and PVA/Al2O3 electrospun mats, Chem. Eng. J. 145 (1) (2008) 169–175.
[27] N. Dharmaraj, C. Kim, H. Kim, Synthesis and characterisation of zirconium oxide nanofibers by electrospinning. Synthesis and Reactivity in Inorganic, Metal-Organic and Nano-Metal Chemistry 36 (1) (2006) 29–32.
[28] C.J. Angammana, S.H. Jayaram, Analysis of the effects of solution conductivity on electrospinning process and fiber morphology, IEEE Trans. Ind. Appl. 47 (3) (2010) 1109–1117.
[29] G. Cadafalch Gazquez, et al., Influence of solution properties and process parameters on the formation and morphology of YSZ and NiO ceramic nanofibers by electrospinning, Nanomaterials 7 (1) (2017) 16.
[30] O. Saligheh, et al., Production and characterization of zirconia (ZrO2) ceramic nanofibers by using electrospun poly (vinyl alcohol)/zirconium acetate nanofibers as a precursor, J. Macromol. Sci., Part B 55 (6) (2016) 605–616.
[31] R.C. Nonato, et al., ZnO micro and nanofibers made by electrospinning: fabrication and characterization, in: 14th IEEE International Conference on Nanotechnology, IEEE, 2014.
[32] L. Shahreen, G.G. Chase, Effects of electrospinning solution properties on formation of beads in TiO2 fibers with PdO particles, Journal of Engineered Fibers and Fabrics 10 (3) (2015), 155892501501000308.
[33] F. Yener, B. Yalcinkaya, Electrospinning of polyvinyl butyral in different solvents, E-Polymers 2013 (1) (2013) 229–242.
[34] G.C. Gazquez, et al., Influence of solution properties and process parameters on the formation and morphology of YSZ and NiO ceramic nanofibers by electrospinning, Nanomaterials 7 (1) (2017) 16.
[35] S. Ramakrishna, et al., An Introduction to Electrospinning and Nanofibers, World Scientific, , Singapore, 2005.
[36] M.M. Demir, et al., Electrospinning of polyurethane fibers. 43 (11) (2002) 3303–3309.
[37] J.-H. He, Y.-Q. Wan, J.-Y. Yu, Application of vibration technology to polymer electrospinning, Int. J. Nonlinear Sci. Numer. Stimul. 5 (3) (2004) 253–262.
[38] A.K. Alves, C.P. Bergmann, F.A. Berutti, Spinger, Novel Synthesis & Characterization of Nanostructured Materials, Engineering Materials, Springer Cham, Berlin, (2013).
[39] X. Yuan, et al., Morphology of ultrafine polysulfone fibers prepared by electrospinning, Polymer Ineternational 53 (11) (2004) 1704–1710.
[40] K.P. Matabola, R.M. Moutloali, The influence of electrospinning parameters on the morphology and diameter of poly(vinyledene fluoride) nanofibers- effect of sodium chloride, J. Mater. Sci. 48 (16) (2013) 5475–5482.
[41] K. Matabola, R. Moutloali, The influence of electrospinning parameters on the morphology and diameter of poly (vinyledene fluoride) nanofibers-effect of sodium chloride, J. Mater. Sci. 48 (16) (2013) 5475–5482.
[42] A. Haider, S. Haider, I.-K. Kang, A comprehensive review summarizing the effect of electrospinning parameters and potential applications of nanofibers in biomedical and biotechnology, Arab. J. Chem. 11 (8) (2018) 1165–1188.
[43] N. Bhardwaj, S.C. Kundu, Electrospinning: a fascinating fiber fabrication technique, Biotechnol. Adv. 28 (3) (2010) 325–347.
[44] A.K. Alves, C.P. Bergmann, F.A. Berutti, Novel synthesis and characterization of nanostructured materials. (2013).
[45] N. Bhardwaj, S.C. Kundu, Electrospinning: a fascinating fiber fabrication technique, Biotechnol. Adv. 28 (3) (2010) 325–347.
[46] T. Sebastian, et al., Synthesis of hydroxyapatite fibers using electrospinning: a study of phase evolution based on polymer matrix, J. Eur. Ceram. Soc. 40 (6) (2020) 2489–2496.